NANO LETTERS

Letter

pubs.acs.org/NanoLett

Exciton Localization and Optical Properties Improvement in Nanocrystal-Embedded ZnO Core−Shell Nanowires

Rui Chen,[†] Quan-Lin Ye,[†,‡] Tingchao He,[†] Van Duong Ta,[†] Yongjun Ying,[†] Yee Yan Tay,[§] Tom Wu,*[,†] and Handong Sun*[,†,⊥]

[†]Division of Physics and Applied Physics, School of Physical and Mathematical Sciences, Nanyang Technological University, Singapore 637371, Singapore

[‡]Department of Physics, Hangzhou Normal University, Hangzhou 310036, P. R. China

[§]Division of Materials Science, School of Materials Science and Engineering and Facility for Analysis, Characterization, Testing, Simulation (FACTS), Nanyang Technological University, Singapore 639798, Singapore

[⊥]Centre for Disruptive Photonic Technologies (CDPT), Nanyang Technological University, Singapore 637371, Singapore

Supporting Information

ABSTRACT: We present a comparative investigation of the morphological, structural, and optical properties of vertically aligned ZnO nanowires (NWs) before and after high energy argon ion (Ar^+) milling. It is found that the outer regions of the as-grown sample change from crystalline to amorphous, and ZnO core−shell NWs with ZnO nanocrystals embedded are formed after Ar^+ milling. Optical properties of the ZnO NWs have been investigated systematically through power and temperature dependent photoluminescence measurements, and the phenomenon of exciton localization as well as the relevant favorable photoluminescence characteristics is elucidated. Interestingly, under high density optical pumping at room temperature, coherent random lasing action is observed, which is ascribed to exciton localization and strong scattering. Our results on the unique optical properties of localized exciton in ZnO core−shell nanostructures shed light on developing stable and high-efficiency excitonic optoelectronic devices such as light-emitting diodes and lasers.

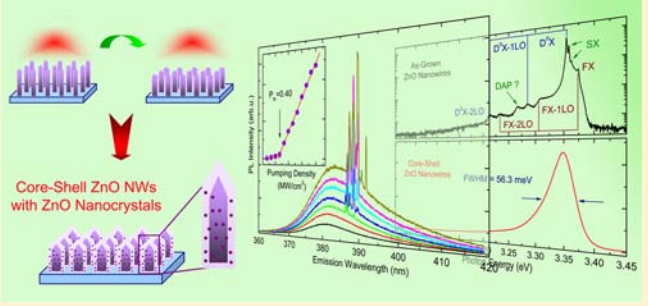

KEYWORDS: *ZnO, photoluminescence, exciton, localization, random lasing*

In recent years, low-dimensional semiconductor structures have attracted extensive research interest.[1−4] Due to the wide direct band gap and large exciton binding energy, ZnO nanomaterials have been recognized as promising candidates to realize short wavelength excitonic devices.[5,6] However, due to the large surface-to-volume ratio, surface states play very important roles on the optical properties of ZnO nanowires (NWs). Generally speaking, the room temperature emission from ZnO NWs always demonstrates a weak near band edge emission in the ultraviolet (UV) region and a broad deep level emission (DLE) in the visible region.[7] The unsatisfactory luminescence efficiency prevents the high device performance. To suppress DLE while enhancing the UV emission of ZnO NWs, various surface modifications such as plasma immersion ion implantation (PIII),[8,9] low energy argon ion (Ar^+) milling,[10] surface plasmon,[11,12] surface passivation,[13] and polymer covering[14,15] have been demonstrated.

Another powerful approach to improving the luminescence efficiency in a semiconductor material is to make use of the optical transitions in localized states, where the oscillator strength is greatly enhanced.[16,17] It has been shown that localized excitons due to the composition fluctuation in InGaN layers significantly improve the performance of optical devices.[18] Moreover, the localized excitons can prevent carrier migration toward nonradiative defects and contribute to the higher optical gain within laser structures because of the enhanced optical efficiency.[16] However, up until now, exciton localization in ZnO nanostructures has rarely been reported, especially for core−shell structure.

Very recently, low energy Ar^+ milling has been adopted to bend ZnO NWs, and it was shown that the sample after low energy Ar^+ treatment exhibits enhanced optical performance due to surface modification. Moreover, the inelastic bending introduces uniaxial tensile strain which enhances the exciton−phonon coupling strength.[10] In the study reported here, the as-grown ZnO NWs were subjected to higher energy Ar^+ beams. It was found that such irradiation changes the morphology of the outer regions of ZnO NWs significantly, from crystalline to amorphous; thus core−shell ZnO NWs were created. The ZnO NWs sample demonstrates very strong exciton localization,

Received: December 2, 2012
Revised: January 12, 2013
Published: January 22, 2013

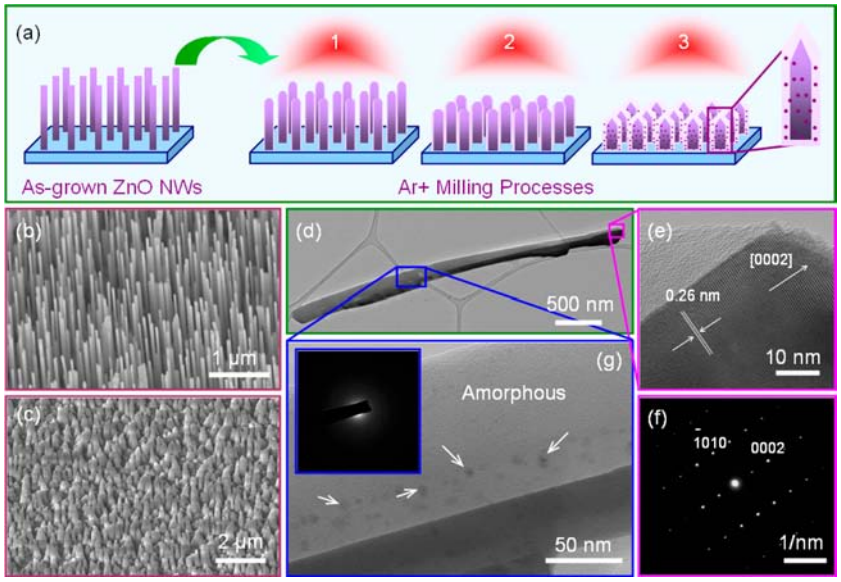

Figure 1. (a) Schematic diagram of the Ar^+ milling processes. (b and c) FESEM image of the ZnO NWs before and after Ar^+ milling. (d) Low-magnification TEM image of the sample after Ar^+ milling. (e) The high-resolution TEM image of the areas at the edge of the sample, and (f) the corresponding SAED pattern. (g) TEM image at the middle part of the sample, where the inset shows the SAED of the amorphous layer. The arrows denote the ZnO nanocrystals.

which was verified by systematic optical measurements. The emission from localized excitons inside ZnO core−shell structures is broad and insensitive to temperature compared to the as-grown sample. Finally, coherent random lasing was observed from the ZnO NWs sample under optical pumping at room temperature, which is ascribed to the higher gain and strong scattering induced by the ZnO nanocrystals emended in amorphous core−shell structures.

The ZnO NWs used herein were fabricated on sapphire substrate using the vapor−liquid−solid technique under optimal growth conditions as reported previously.[19,20] Ar^+ milling of the sample was carried out in a high vacuum chamber equipped with an ion source. During the 15 min milling process, the ion beam energy was fixed at 1 keV with a beam current of 90 mA. A JEOL JSM-7001F field emission scanning electron microscope (FESEM) was used to characterize the morphology of the sample. The transmission electron microscopy (TEM) measurement was performed at the Facility for Analysis, Characterization, Testing and Simulation (FACTS) in Nanyang Technological University, Singapore, where a JEOL 2100F with a field emission gun source was used. The photoluminescence (PL) measurements were performed between 10 and 300 K within a helium closed-cycle cryostat. A He−Cd laser with laser line of 325 nm was used as the excitation source, and the signal was dispersed by a 750 mm monochromator combined with suitable filters and detected by a photomultiplier using the standard lock-in amplifier technique. For high density excitation, the signal was collected using the same system, but the excitation source was replaced by a pulsed Nd:YAG fourth harmonic (266 nm) laser and detected by a UV-enhanced charged coupled device (CCD). The pulse width and repetition rate of the laser are about 1 ns and 60 Hz, respectively.

Figure 1a schematically shows the formation of ZnO core−shell structure by Ar^+ milling. The as-grown vertically aligned ZnO NWs were subjected to high energy Ar^+ beams perpendicular to the sample surface. As the time increases, the ZnO NWs were pared, and an amorphous layer was created at the outer region with plenty of ZnO nanocrystals embedded. This is evident by the FESEM images, as shown in Figure 1b,c, where the vertically aligned as-grown sample becomes much shorter and transforms into a core−shell structure. The structure of the samples was further analyzed by TEM, and the typical low-magnification image of the sample after Ar^+ milling was presented in Figure 1d. It is noted that the modified NW shows different contrasts in some local regions. The high-resolution TEM image at the edge of the NW is shown in Figure 1e. Well-defined lattice fringes with an interplanar *d*-spacing of 0.26 nm can be indexed as ZnO [0002] plane, with a preferential orientation in the *c*-axis direction.[21] The corresponding selected area electron diffraction (SAED) pattern shown in Figure 1f supports the wurtzite nature of ZnO. However, it is interesting to observe a broad diffuse SAED pattern at the outer layer of ZnO as shown in Figure 1g, which implies that this layer is amorphous. It is also found that the entire outer regions of the sample were covered by amorphous ZnO layer and formed a core−shell structure. A closer look at the structure reveals that there are numbers of nanocrystals with size ∼5 nm embedded in the amorphous matrix, as denoted by the arrows in Figure 1g. Compared to the as-grown sample, the morphology change of ZnO from crystalline to amorphous should be ascribed to the Ar^+ milling due to the high ion beam energy and long milling time.

Figure 2 plots the room temperature PL spectrum of the ZnO NWs before and after Ar^+ milling. Near band edge emission and DLE can be observed from the as-grown NWs. However, it is interesting to note that, after Ar^+ milling, the UV emission is enhanced by a factor of around 3.25, while the visible DLE is totally suppressed. The reason of this will be explained later. From the normalized UV region spectrum shown in the inset of Figure 2, it can be seen that the near band edge emission from the sample after Ar^+ milling was located at 3.280 eV, with a redshift of 11 meV compared to the as-grown ZnO NWs positioned at 3.291 eV. The redshift of the emission peak implies that quantum confinement effect does not play any role in our material system. At the same time, it is noted

dx.doi.org/10.1021/nl304433m | *Nano Lett.* 2013, 13, 734−739

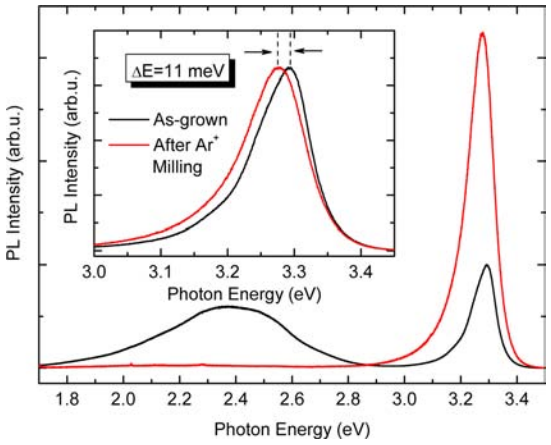

Figure 2. Room temperature PL spectra of the ZnO NWs before and after Ar^+ milling. The inset shows the normalized close-up image of the PL spectra in the UV region.

that the bandwidth of the emission increases after Ar^+ milling. Similar phenomena have been observed before and was ascribed to various reasons such as the laser heating effect,[22] the presence of uniaxial stress/strain,[23,24] and the contributions of excitonic emission and their phonon replicas.[25,26] However, as will be discussed later, all of the existing explanations cannot account for our observation here.

The low-temperature (10 K) PL spectra of the ZnO NWs before and after Ar^+ milling are depicted in Figure 3a and b, respectively. As can be seen in Figure 3a, the emission from the as-grown ZnO NWs at 10 K is dominated by radiative recombination from neutral donor-bound excitons (D^0X) located at 3.355 eV. At the higher energy region, two peaks at 3.359 and 3.363 eV may due to recombination of donor-like surface excitons (SX).[8,27,28] The peak at 3.374 eV comes from the free exciton (FX) emission. It is also straightforward to identify the longitudinal optical (LO) phonon replicas of D^0X and FX as shown in the figure.[29] Moreover, at ~3.267 eV, a small peak can be observed, which may be related to the recombination of donor−acceptor pair (DAP).[30] Compared to the as-grown sample, the modified ZnO NWs only shows a broad emission located at 3.347 eV, with a full width at half-maximum (fwhm) as large as 56.3 meV. There is no apparent LO phonon replicas in the core−shell ZnO NWs, which points out the weak exciton−phonon coupling strength. More interestingly, the FX emission does not exist in the sample. To better understand the origin of the emission from ZnO NWs, we adjusted the excitation power by 2 orders of magnitude, and the corresponding PL spectrum is plotted in Figure 3c. It can be seen that, under different excitation densities, the shape and position of the emission remain unchanged. From Figure S1 as shown in the Supporting Information, it is noted that the bandwidth of the emission increases monotonically with excitation density. Such a "band filling" effect suggests the PL feature of localized states as will be clarified subsequently. The integrated PL intensity of emission under different excitation densities is shown in Figure 3d. The integrated PL intensity (I_{PL}) can be described by a function related to the excitation laser power (I_{EX}) as $I_{PL} \propto I_{EX}^{\alpha}$,[31] where α is the nonlinear component. It can be seen that the integrated PL intensity of ZnO NWs increases approximately linearly with the excitation density. By fitting the experimental data, a value of 0.96 of the component α can be

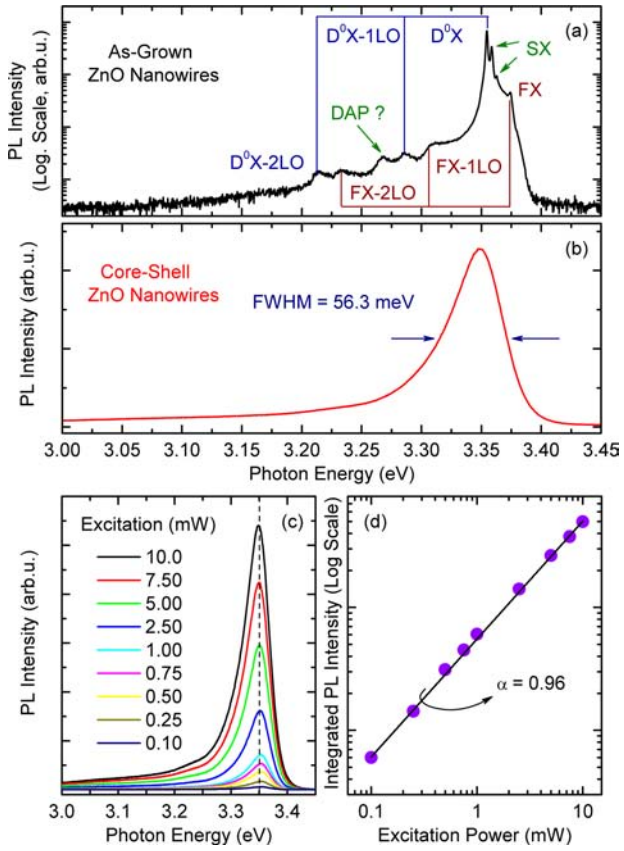

Figure 3. (a and b) Low temperature (10 K) PL spectrum of the ZnO NWs before and after Ar^+ milling. (c) The PL spectra of core−shell ZnO NWs under different power densities. (d) The relationship between the integrated PL intensity and the excitation power.

obtained, which indicates that the transition in the modified ZnO NWs is related to excitonic emission.

It is known that the optical properties of semiconductors are strongly influenced by disorder due to interface roughness, defects, and/or strain. As can be seen from Figure 1g, the whole outer part of the NW is covered by amorphous layers after Ar^+ milling. There are plenty of ZnO nanocrystals embedded in the core−shell structure, which will introduce many localized states. Therefore, instead of sharp conduction and valence band edges, exponential tails may be left in the electronic density of states (DOS). As can be seen in Figure 3b, the low temperature PL spectrum is broad and asymmetric in the low energy side, which verify the existence of localized states. It is worthwhile to mention that the excitation wavelength used herein for PL measurement is 325 nm, and the penetration depth is around 100 nm for ZnO.[32] Therefore, even with the inhomogeneous amorphous ZnO shell, part of the crystalline ZnO core can still absorb photons under optical excitation. However, no FX emission from the crystalline core can be observed; thus it is reasonable to deduce that excitons generated in the core region transfer their energy to the localized states and contribute to the emission. This is supported by Figure 1g, where the ZnO nanocrystals are located near the boundaries of the crystalline ZnO core materials. Due to the lower energy level of the localized states and the size inhomogeneity of ZnO nanocrystals, emission from the core−shell structure is red-shifted and broadened compared to the as-grown one (as depicted in the inset of Figure 2). For ZnO NWs with a large surface-to-volume ratio, the general consensus for the ZnO green DLE is

dx.doi.org/10.1021/nl304433m | Nano Lett. 2013, 13, 734−739

from oxygen vacancies near the surface.[9,33] In our experiment, after high energy Ar^+ milling, the ZnO NWs become shorter and thinner; therefore the quenching of the DLE can be ascribed to the passivation effect. Meanwhile, strong exciton localization can improve the emission efficiency by preventing migration of excitons toward nonradiative defects. This is the reason why the optical property of the ZnO NWs is significantly improved after the Ar^+ milling.

Further evidence of exciton localization in core−shell ZnO NWs is witnessed by temperature-dependent PL measurement performed between 10 and 300 K. As shown in Figure 4a, the

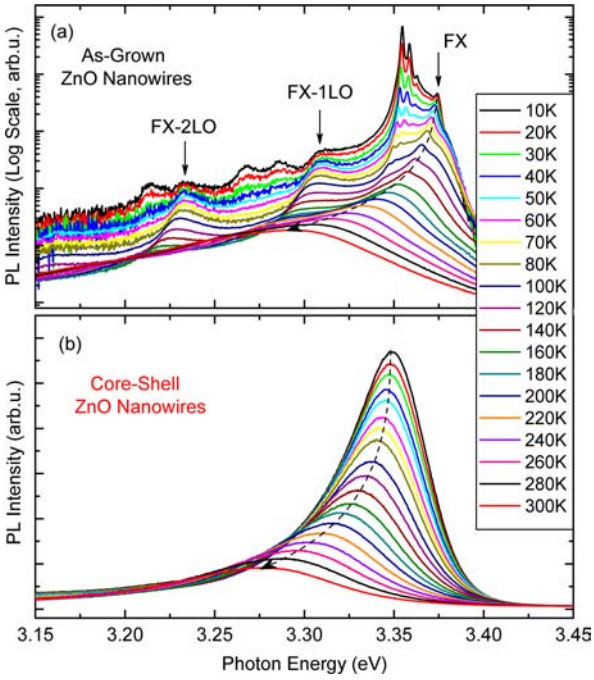

Figure 4. Temperature-dependent PL spectra of the ZnO NWs before and after Ar^+ milling. The dashed lines denote the evolution of the exciton emissions.

emission intensity of D^0X and SX decreases quickly on warming and totally disappears at temperature ~100 K. The emission peak of FX demonstrates a gradual redshift with temperature, and the room temperature emission is dominated by FX with its phonon replicas. In comparison, the emission from core−shell ZnO NWs shows single-peak emission up to room temperature, as can be seen in Figure 4b. It is noted that the fwhm of the emission increases with temperature, which can be ascribed to the exciton diffusion between different localized states at higher temperature. More information about the comparison of PL spectra of the as-grown ZnO NWs, bent ZnO NWs, and core−shell ZnO NWs at different temperatures can be found in Figure S2 in the Supporting Information.

To better understand the temperature-dependent optical property of the sample, emission peak position and intensity of the ZnO NWs before and after Ar^+ milling were presented in Figure 5a and b, respectively. As shown in Figure 5a, the photon energy of FX of the as-grown ZnO NWs decreases monotonically as temperature increases, which can be well-fitted by the empirical Varshni's equation.[34] The band gap energy obtained from the fitting is 3.3745 eV, which is consistent with the reported data of free exciton A.[35] Comparatively, for the emission from core−shell ZnO NWs

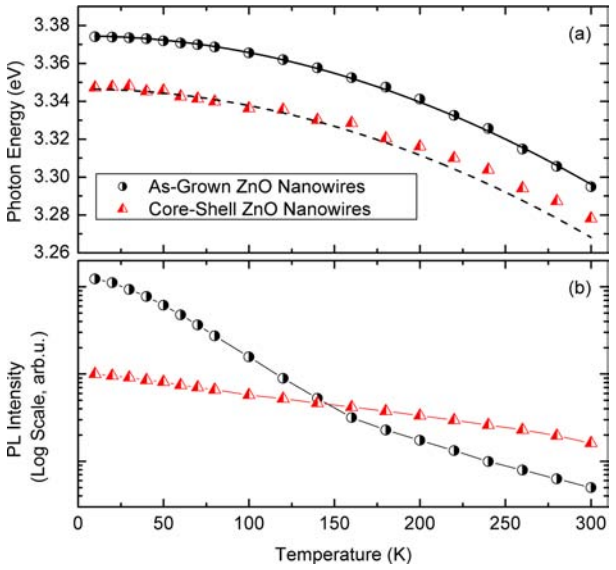

Figure 5. (a) The emission photon energy of the ZnO NWs before and after Ar^+ milling. The solid line is the fitting to the Varshni's equation, while the dashed line shifts down from the solid line by 28 meV. (b) The emission intensities of the samples change with temperature.

sample as depicted in Figure 5a, the emitted photon energy is always lower than the FX emission from the as-grown sample. Moreover, it is noted that the peak energy difference between two samples decreases as temperature increases. This suggests that the PL from core−shell ZnO NWs is not dominated by the FX emission but from localized excitons. At higher temperatures, the increased thermal energy may be sufficient to detrap carriers from localized states and reveal more features of FX recombination.[36,37] However, it is needed to mention that the degree of localization in core−shell ZnO NWs is so strong that the excitons do not have enough thermal energy to dissociate even at room temperature. Thanks to the strong exciton localization, the emission intensity from the core−shell ZnO NWs is not sensitive to temperature, as can be seen from Figure 5b. For the case of as-grown ZnO NWs, the PL intensity of the FX emission decreases more than 2 orders of magnitudes for temperature increasing from 10 to 300 K. However, it can be seen that the emission intensity from core−shell ZnO NWs is very stable, changing only about six times under the identical temperature range. Therefore, we can conclude that the amorphous ZnO covering and the strong localization in ZnO nanocrystals greatly suppress the surface trapping and nonradiative exciton recombination process, which enables broad and temperature-insensitive excitonic emission from ZnO. Such kinds of materials should be very useful for high-performance optoelectronic device applications.

We also examined the emission of the sample under high density optical pumping by a pulse laser. Figure 6a shows the PL spectra of the sample after Ar^+ milling under different pumping densities at room temperature. It can be seen that the sample displays a weak spontaneous emission under low pumping density. When the pumping density exceeds a threshold of ~0.40 MW/cm^2, sharp peaks emerge from the low energy shoulder of the broad spontaneous emission. As the pumping density further increases, multiple spikes ~389 nm can be detected, the intensity of which increases rapidly. A plot of integrated PL intensity of these stimulated peaks with respect

dx.doi.org/10.1021/nl304433m | Nano Lett. 2013, 13, 734−739

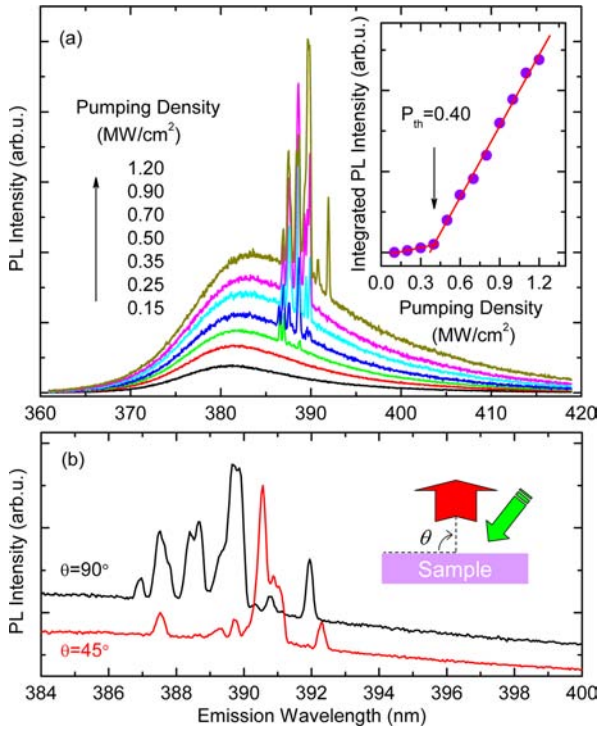

Figure 6. (a) Room-temperature random lasing from core−shell ZnO NWs under optical pumping. The inset shows the integrated PL intensity of all the sharp peaks with pumping density. (b) The emission spectra of core−shell ZnO NWs detected at two different observation angles, and the inset shows the measurement configuration.

to pumping density is given in the inset of Figure 6a. Such a nonlinear increase of the integrated intensity is a characteristic of lasing. It is known that the lasing action requires proper optical feedback. For the sample discussed herein, the optical feedback should be realized by random scattering, because the asymmetric shape of the sample (as shown in Figure 1c) is difficult to support either Fabry-Pérot[1,38,39] or whispering gallery mode cavity.[40−42] To clarity the lasing mechanism, angle-dependent PL measurements were carried, and the results were plotted in Figure 6b. It is clearly seen that different emission spectra can be recorded from different directions, which is qualitatively consistent with the random lasing behavior with coherent feedback.[43−45] Therefore, it is concluded that the lasing action can be classified to random lasing.

Compared with the core−shell ZnO NWs, the as-grown ZnO NWs only exhibit broad spontaneous emission under identical conditions (data not shown here). It is well-known that the DOS of the localized states is lower than that of the extended band states, which means that it can be easier occupied by the moderate pumping.[16] If the optical gain coming from the filled localized states exceeds the light propagation loss, stimulated emission will happen. This phenomenon has been observed in II−VI compound semiconductors.[46,47] At the same time, the ZnO nanocrystals inside the core−shell structure will serve as scattering centers and introduce strong scattering. Therefore, the observation of random lasing action is ascribed to the strong exciton localization and scattering due to ZnO nanocrystals. Up till now, various material growth approaches and post-treatments are devoted to achieve strong FX emission in ZnO material. Herein, we provided the proof-of-concept demonstration of the unique optical properties of localized exciton in ZnO nanomaterials. It can be seen that the strong exciton localization in ZnO nanocrystals not only enables the broad, temperature-insensitive excitonic emission, but also provides higher gain for lasing, which should be useful for high performance optoelectronic device applications or random lasing even from single NW.

In summary, we have investigated the morphology and optical property of ZnO NWs before and after high energy Ar^+ milling. It was found that Ar^+ milling effectively passivated the DLE of ZnO and enhanced the UV emission simultaneously. From systematic optical measurements, the observation was ascribed to the existence of strong exciton localization induced by Ar^+ milling. The excitonic emission from the core−shell ZnO NWs was more broad and stable compared to the as-grown ZnO NWs, and the mechanism was discussed in detail. Furthermore, random lasing action was observed from the core−shell ZnO NWs under optical pumping at room temperature, which was ascribed to exciton localization and strong scattering. Our investigations demonstrate the unique optical properties of localized exciton in ZnO hybrid amorphous/crystalline nanomaterials, highlighting the importance of structure−property correlation and their potential device applications.

■ ASSOCIATED CONTENT

Supporting Information

Low-temperature spectrum bandwidth of the emission from core−shell ZnO NWs with different excitation densities, and comparison of emission from the as-grown ZnO NWs, bent ZnO NWs (data from ref 10), and core−shell ZnO NWs at various temperatures. This material is available free of charge via the Internet at http://pubs.acs.org.

■ AUTHOR INFORMATION

Corresponding Author

*E-mail: tomwu@ntu.edu.sg and hdsun@ntu.edu.sg.

Notes

The authors declare no competing financial interest.

■ ACKNOWLEDGMENTS

Support from the Singapore Ministry of Education through the Academic Research Fund (Tier 1) under Project No. RG63/10 and from the Singapore National Research Foundation through the Competitive Research Programme (CRP) under Project No. NRF-CRP5-2009-04 and NRF-CRP6-2010-02 is gratefully acknowledged.

■ REFERENCES

(1) Huang, M. H.; Mao, S.; Feick, H.; Yan, H. Q.; Wu, Y. Y.; Kind, H.; Weber, E.; Russo, R.; Yang, P. D. *Science* **2001**, *292*, 1897−1899.
(2) Law, M.; Greene, L. E.; Johnson, J. C.; Saykally, R.; Yang, P. *Nat. Mater.* **2005**, *4*, 455−459.
(3) Chen, R.; Li, D.; Liu, B.; Peng, Z.; Gurzadyan, G. G.; Xiong, Q.; Sun, H. D. *Nano Lett.* **2010**, *10*, 4956−4961.
(4) Chen, R.; Xing, G. Z.; Gao, J.; Zhang, Z.; Wu, T.; Sun, H. D. *Appl. Phys. Lett.* **2009**, *95*, 061908.
(5) Tang, Z. K.; Wong, G. K. L.; Yu, P.; Kawasaki, M.; Ohtomo, A.; Koinuma, H.; Segawa, Y. *Appl. Phys. Lett.* **1998**, *72*, 3270−3272.
(6) Zhang, B. P.; Binh, N. T.; Wakatsuki, K.; Segawa, Y.; Yamada, Y.; Usami, N.; Kawasaki, M.; Koinuma, H. *Appl. Phys. Lett.* **2004**, *84*, 4098−4100.

(7) Zeng, H.; Duan, G.; Li, Y.; Yang, S.; Xu, X.; Cai, W. *Adv. Funct. Mater.* **2010**, *20*, 561−572.
(8) Yang, Y.; Tay, B. K.; Sun, X. W.; Sze, J. Y.; Han, Z. J.; Wang, J. X.; Zhang, X. H.; Li, Y. B.; Zhang, S. *Appl. Phys. Lett.* **2007**, *91*, 071921.
(9) Yang, Y.; Sun, X. W.; Tay, B. K.; Cao, P. H. T.; Wang, J. X.; Zhang, X. H. *J. Appl. Phys.* **2008**, *103*, 064307.
(10) Chen, R.; Ye, Q.-L.; He, T. C.; Wu, T.; Sun, H. D. *Appl. Phys. Lett.* **2011**, *98*, 241916.
(11) Hwang, S. W.; Shin, D. H.; Kim, C. O.; Hong, S. H.; Kim, M. C.; Kim, J.; Lim, K. Y.; Kim, S.; Choi, S.-H.; Ahn, K. J.; Kim, G.; Sim, S. H.; Hong, B. H. *Phys. Rev. Lett.* **2010**, *105*, 127403.
(12) Shao, D.; Sun, H.; Yu, M.; Lian, J.; Sawyer, S. *Nano Lett.* **2012**, *12*, 5840−5844.
(13) Lin, C.-C.; Chen, H.-P.; Liao, H.-C.; Chen, S.-Y. *Appl. Phys. Lett.* **2005**, *86*, 183103.
(14) Liu, K. W.; Chen, R.; Xing, G. Z.; Wu, T.; Sun, H. D. *Appl. Phys. Lett.* **2010**, *96*, 023111.
(15) Richters, J.-P.; Voss, T.; Wischmeier, L.; Ruckmann, I.; Gutowski, J. *Appl. Phys. Lett.* **2008**, *92*, 011103.
(16) Satake, A.; Masumoto, Y.; Miyajima, T.; Asatsuma, T.; Nakamura, F.; Ikeda, M. *Phys. Rev. B* **1998**, *57*, R2041−R2044.
(17) O'Donnell, K. P.; Martin, R. W.; Middleton, P. G. *Phys. Rev. Lett.* **1999**, *82*, 237−240.
(18) Florescu, D. I.; Ramer, J. C.; Lee, D. S.; Armour, E. A. *Appl. Phys. Lett.* **2004**, *84*, 5252−5254.
(19) Xing, G.; Wang, D.; Yi, J.; Yang, L.; Gao, M.; He, M.; Yang, J.; Ding, J.; Sum, T. C.; Wu, T. *Appl. Phys. Lett.* **2010**, *96*, 112511.
(20) Zhang, Z.; Wang, S. J.; Yu, T.; Wu, T. *J. Phys. Chem. C* **2007**, *111*, 17500−17505.
(21) Chen, R.; Tay, Y. Y.; Ye, J.; Zhao, Y.; Xing, G. Z.; Wu, T.; Sun, H. D. *J. Phys. Chem. C* **2010**, *114*, 17889−17893.
(22) Yang, Y.; Yan, H.; Fu, Z.; Yang, B.; Xia, L.; Xu, Y.; Zuo, J.; Li, F. *J. Phys. Chem. B* **2005**, *110*, 846−852.
(23) Yan, B.; Chen, R.; Zhou, W. W.; Zhang, J. X.; Sun, H. D.; Gong, H.; Yu, T. *Nanotechnology* **2010**, *21*, 445706.
(24) Han, X.; Kou, L.; Lang, X.; Xia, J.; Wang, N.; Qin, R.; Lu, J.; Xu, J.; Liao, Z.; Zhang, X.; Shan, X.; Song, X.; Gao, J.; Guo, W.; Yu, D. *Adv. Mater.* **2009**, *21*, 4937−4941.
(25) Voss, T.; Bekeny, C.; Wischmeier, L.; Gafsi, H.; Borner, S.; Schade, W.; Mofor, A. C.; Bakin, A.; Waag, A. *Appl. Phys. Lett.* **2006**, *89*, 182107.
(26) Ahn, C. H.; Mohanta, S. K.; Lee, N. E.; Cho, H. K. *Appl. Phys. Lett.* **2009**, *94*, 261904.
(27) Fallert, J.; Hauschild, R.; Stelzl, F.; Urban, A.; Wissinger, M.; Zhou, H.; Klingshirn, C.; Kalt, H. *J. Appl. Phys.* **2007**, *101*, 073506.
(28) Wischmeier, L.; Voss, T.; Ruckmann, I.; Gutowski, J.; Mofor, A. C.; Bakin, A.; Waag, A. *Phys. Rev. B* **2006**, *74*, 195333.
(29) Sun, H. D.; Segawa, Y.; Kawasaki, M.; Ohtomo, A.; Tamura, K.; Koinuma, H. *J. Appl. Phys.* **2002**, *91*, 6457−6460.
(30) Teke, A.; Özgür, Ü.; Doğan, S.; Gu, X.; Morkoç, H.; Nemeth, B.; Nause, J.; Everitt, H. O. *Phys. Rev. B* **2004**, *70*, 195207.
(31) Bergman, L.; Chen, X.-B.; Morrison, J. L.; Huso, J.; Purdy, A. P. *J. Appl. Phys.* **2004**, *96*, 675−682.
(32) Pan, C. J.; Tu, C. W.; Song, J. J.; Cantwell, G.; Lee, C. C.; Pong, B. J.; Chi, G. C. *J. Cryst. Growth* **2005**, *282*, 112−116.
(33) Rosenberg, R. A.; Haija, M. A.; Vijayalakshmi, K.; Zhou, J.; Xu, S.; Wang, Z. L. *Appl. Phys. Lett.* **2009**, *95*, 243101.
(34) Varshni, Y. P. *Physica (Amsterdam)* **1967**, *34*, 149−154.
(35) Reynolds, D. C.; Look, D. C.; Jogai, B.; Litton, C. W.; Collins, T. C.; Harsch, W.; Cantwell, G. *Phys. Rev. B* **1998**, *57*, 12151−12155.
(36) Chen, R.; Phann, S.; Sun, H. D.; Zhuang, Q.; Godenir, A. M. R.; Krier, A. *Appl. Phys. Lett.* **2009**, *95*, 261905.
(37) Sun, H. D.; Hetterich, M.; Dawson, M. D.; Egorov, A. Y.; Bernklau, D.; Riechert, H. *J. Appl. Phys.* **2002**, *92*, 1380−1385.
(38) Johnson, J. C.; Yan, H.; Schaller, R. D.; Haber, L. H.; Saykally, R. J.; Yang, P. *J. Phys. Chem. B* **2001**, *105*, 11387−11390.
(39) Chen, R.; Sun, H. D.; Wang, T.; Hui, K. N.; Choi, H. W. *Appl. Phys. Lett.* **2010**, *96*, 241101.
(40) Czekalla, C.; Nobis, T.; Rahm, A.; Cao, B.; Zúñiga-Pérez, J.; Sturm, C.; Schmidt-Grund, R.; Lorenz, M.; Grundmann, M. *Phys. Status Solidi B* **2010**, *247*, 1282−1293.
(41) Dai, J.; Xu, C. X.; Zheng, K.; Lv, C. G.; Cui, Y. P. *Appl. Phys. Lett.* **2009**, *95*, 241110.
(42) Chen, R.; Ling, B.; Sun, X. W.; Sun, H. D. *Adv. Mater.* **2011**, *23*, 2199−2204.
(43) Cao, H.; Zhao, Y. G.; Ho, S. T.; Seelig, E. W.; Wang, Q. H.; Chang, R. P. H. *Phys. Rev. Lett.* **1999**, *82*, 2278−2281.
(44) Cao, H. *Waves Random Media* **2003**, *13*, R1−R39.
(45) Chen, R.; Bakti Utama, M. I.; Peng, Z.; Peng, B.; Xiong, Q.; Sun, H. D. *Adv. Mater.* **2011**, *23*, 1404−1408.
(46) Yamada, Y.; Masumoto, Y.; Mullins, J. T.; Taguchi, T. *Appl. Phys. Lett.* **1992**, *61*, 2190−2192.
(47) Ding, J.; Jeon, H.; Ishihara, T.; Hagerott, M.; Nurmikko, A. V.; Luo, H.; Samarth, N.; Furdyna, J. *Phys. Rev. Lett.* **1992**, *69*, 1707−1710.